Electrochemical and Solid-State Letters, **11** (6) A94-A96 (2008)
1099-0062/2008/11(6)/A94/3/$23.00 © The Electrochemical Society

Ab Initio Study of the Surface Properties and Nanoscale Effects of $LiMnPO_4$

L. Wang, F. Zhou, and G. Ceder*,z

Department of Materials Science and Engineering, Massachusetts Institute of Technology, Cambridge, Massachusetts 02139, USA

Using first-principles calculations, we investigate the surface energies, equilibrium morphology, and surface redox potentials for $LiMnPO_4$ in the olivine structure. Low-energy surfaces are found in the [100], [010], [011], [101], [201], and [301] directions of the orthorhombic structure. With the calculated surface energies, we provide the thermodynamic equilibrium shape for the $LiMnPO_4$ crystal through a Wulff construction. The dominating surfaces in the Wulff shape are (010), (011), and (201). Most of the surfaces in the Wulff shape have lower Li extraction potentials than the bulk, except for the (100) and (011) surfaces.
 [DOI: 10.1149/1.2901974]

Manuscript submitted January 28, 2008; revised manuscript received February 28, 2008. Available electronically April 3, 2008.

$LiMnPO_4$ with the olivine structure can be an ideal substitute for the commonly used cathode material $LiCoO_2$ due to its equilibrium voltage of 4.1 V, which is compatible with the electrolyte presently used in Li-ion batteries. While it has a lower density leading to a lower energy density, its safety, like that of other lithium transition metal phosphates, is probably much better than that of $LiCoO_2$. Unfortunately, its electrochemical performance, even at a reasonable current rate, is not good.[1-5] There is still debate why $LiMnPO_4$ has a poor electrochemical performance. Various possible explanations, such as the lack of existence of a pure fully delithiated phase $MnPO_4$ in the olivine structure,[6] the intrinsically low electronic conductivity,[2] the slow lithium diffusion kinetics within $MnPO_4$,[7] and the large coherent strain between $LiMnPO_4$ and $MnPO_4$,[8] have been proposed. The most effective experimental approach reported previously is the use of small particles to improve its rate performance.[2,3,7] This is largely stimulated by the belief that a decrease in the particle size yields a decrease in Li and/or electron transport length and an increase in the relative surface area. However, considering that Li diffusion in the phosphates is one-dimensional and restricted to the [010] direction of the olivine structure,[9] morphology control with the objective of reducing the particle thickness in the [010] direction and maximizing the active (010) surface area can be more effective to improve the electrochemical performance of $LiMnPO_4$. Thus, a plate-type particle shape with a reduced thickness in the [010] direction can be more beneficial than a spherical particle of the same volume. For a crystal in its equilibrium shape, the relative area of each facet on a particle depends on its surface energy. We recently used first-principles methods to determine the surface energy and redox potential of various surfaces of $LiFePO_4$, and found that the low energy of the (010) surface makes it contribute significantly to the total equilibrium surface area of a particle.[10] At present, experimental or computed data on the surface energetics and equilibrium particle morphology of $LiMnPO_4$ are not available. Surfaces are also important for the perturbation that they may cause in the voltage curve. While for bulk materials the surface effect on the charge/discharge thermodynamics is negligible, for nanoparticles, the region influenced by the surface may become a significant fraction of the total amount of Li sites. For $LiFePO_4$, the (010) surface has a Li redox potential much lower than the bulk value, while most of the surfaces that are orthogonal to the (010) surface, e.g., the (100) and (201) surfaces, have a Li redox potential higher than the bulk value.[10] The variations in the surface Li redox potentials will lead to the inhomogeneous delithiation/lithiation of nanoscale $LiFePO_4$ particles: For voltages between the (010) surface potential (about 2.9–3.0 V) and that of bulk $LiFePO_4$, a region extending from the (010) surface will be delithiated while the bulk is not. While the extent of this region is currently not known, one can expect it to be several layers due to the phase-separating nature of $LiFePO_4$ and $FePO_4$.[11] Similarly, the surfaces with a potential above that of bulk $LiFePO_4$ will create a lithiated region extending from these surfaces even when the bulk of the material is delithiated. Laffont et al.'s recent findings[12] on Li insertion/extraction from plate-type nano-$LiFePO_4$ with a large (010) surface area are consistent with our model. They found that the $LiFePO_4$-to-$FePO_4$ phase transition initially occurs at the center region on the (010) plane of the plate-type particle, and the $FePO_4$-to-$LiFePO_4$ conversion first takes place at the peripheral region of the particle. This inhomogeneous Li insertion/extraction for the well-faceted nano-$LiFePO_4$ is unexpected, and it is not clear whether this behavior is universally true for all phosphates. In this work, we will therefore study the surface energies, equilibrium shape, and surface Li redox potentials for $LiMnPO_4$.

Methodology

We used a first-principles electronic structure technique, with the generalized gradient approximation (GGA) to density functional theory. The projected augmented wave[13] method was used, as implemented in the Vienna ab initio simulation package.[14] Electron correlation within the d states significantly affects the electronic structure and energetic properties of transition metal oxides.[15,16] In this work, the GGA + U approach[17,18] was used to accurately calculate the surface redox potentials. We employed the rotational invariant scheme as presented by Dudarev,[19] and chose a J value of 1 eV and a U value of 5.5 eV, which is the average of the self-consistently calculated U values for Mn^{2+} (U = 4.9 eV in $LiMnPO_4$) and Mn^{3+} (U = 6.1 eV in $MnPO_4$) in the olivine structure.[16] A ferromagnetic high-spin Mn state was assumed.

Bulk $LiMnPO_4$ has an orthorhombic structure with a space group of *Pnma*. The calculated lattice parameters of the fully relaxed bulk structure were a = 10.5630 Å, b = 6.1725 Å, and c = 4.7959 Å, in good agreement with experiments.[20] The initial, unrelaxed, surface structures were carved out from the fully relaxed bulk crystal. In this study, we only considered surfaces that leave the crystal stoichiometric. The surface structures of $LiMnPO_4$ were created following the same principles as summarized in the Methodology section of Ref. 10.

All calculations were performed on a slab model[21] with the lattice parameter of the supercell and the slab fixed at its bulk value, and only atoms near the surface were allowed to relax until the forces on them were smaller than 0.03 eV/Å. The inner part of the slab was frozen at the bulk position to simulate the bulk of $LiMnPO_4$. More computational details about the thickness of the vacuum, slab, and free relaxation layer in each direction can be found in our previous paper.[10] We estimate the computational error in the calculated surface energies to be less than 5%. The equilibrium shape of a crystal is related to the surface energies through the Wulff construction.[22] Note that only planes that are part of the Wulff shape are thermodynamically stable.

* Electrochemical Society Active Member.
z E-mail: gceder@mit.edu

Table I. Calculated surface energies γ (in units of J/m^2) of $LiMnPO_4$ in 15 directions and surface redox potentials Φ (in units of volts) of $LiMnPO_4$ in six directions. Surface energies and surface redox potentials of $LiFePO_4$ taken from Ref. 10 are also provided for comparison.

Directions	(100)	(010)	(001)	(011)	(101)	(110)	(111)	(012)	(021)	(102)	(201)	(120)	(210)	(301)	(401)
γ of $LiMnPO_4$	0.66	0.67	1.04	0.67	0.65	1.36	0.81	1.20	0.88	1.11	0.55	1.01	0.87	0.67	1.23
Φ of $LiMnPO_4$	4.18	3.20		4.09	3.70						3.86		3.76		
γ of $LiFePO_4$	0.66	0.64	0.97	0.76	0.62	1.30	0.85				0.52			0.62	1.15
Φ of $LiFePO_4$	3.84	2.95		3.79	3.25						3.76				

To calculate the surface Li redox potentials, all the Li atoms on the top (and also symmetrically equivalent Li atoms on the bottom) layer of each surface slab were extracted. The reader can refer to Fig. 2–9 in Ref. 10 for details about the locations and amounts of Li atoms extracted from different surfaces.

Results

Surface energies.— We investigate surface energies in 13 low-index directions with components of the Miller index lower than 2, plus two high-index directions. For each orientation, different surface terminations are considered and only the lowest value of surface energy is reported here. As summarized in Table I, the calculated surface energies are in the range of 0.55–1.36 J/m^2. The relative low-energy surfaces are (100), (010), (011), (101), (201), and (301). However, the values of surface energies in these six directions are not significantly different from each other.

Wulff shape.— The Wulff shape for $LiMnPO_4$ based on the surface energies in Table I is shown in Fig. 1. A gray-scale (color online) scheme is used, with the lighter surfaces indicating lower surface energy. Only 6 of the 15 surfaces that we considered appear in the Wulff shape. The other surfaces are not stable against combinations of the six facets. The (301) surface is calculated to be low in energy but is not stable with respect to the formation of faceting by (201) and (100) facets. The (010), (011), and (201) surfaces dominate in the Wulff shape of $LiMnPO_4$. These three surfaces contribute about 87% of the total surface area in Fig. 1. The Wulff shape is truncated by the (101) surface in the [001] direction and capped by the (100) facet.

Surface redox potentials.— It is of interest to compare the redox potentials to extract Li from various surfaces. In this study, we calculate the Li redox potentials only for the six surfaces that appear in our Wulff shape, as they are likely to be the most important ones. Note that the calculated surface redox potentials should be interpreted as the average redox potential to extract/insert Li from/into the outermost layer of a given surface. The results are provided in Table I and Fig. 1 (see the numbers beside the Miller indexes). The surface potentials range from 3.20 to 4.18 V, compared to the calculated Li insertion/extraction redox potential of 4.00 V in the bulk. The bulk redox potential is consistent with previous work[16] and is within a few percent of the experimental voltage (4.1 V).[20] All surfaces, except for (100) and (011), have a redox potential lower than the bulk value. The (010) surface has the lowest surface redox potential of 3.20 V. For comparison, Table I also lists the surface voltages of $LiFePO_4$ taken from Ref. 10.

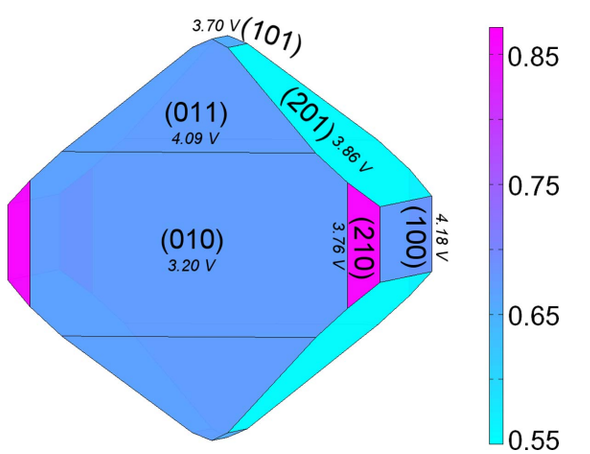

Figure 1. (Color online) Wulff shape of $LiMnPO_4$ using the calculated surface energies in 15 directions. The gray-scale bar on the right gives the energy scale of the surface in units of J/m^2. The numbers below the Miller indexes provide the redox potential to extract Li at that surface.

Discussion

Surface energy and Wulff shape difference between $LiMnPO_4$ and $LiFePO_4$.— We can see from Table I that the surface energies of $LiMnPO_4$ are relatively low in the following six orientations: (100), (010), (011), (101), (201), and (301). The first five surfaces appear in the Wulff shape of $LiMnPO_4$, together with the (210) surface. To compare the surface energies of $LiFePO_4$ and $LiMnPO_4$, we also include in Table I the values that we previously obtained for $LiFePO_4$.[10] The six lowest energy surfaces for $LiMnPO_4$ and $LiFePO_4$ are the same (though not in the same order). Moreover, the surface energies for $LiMnPO_4$ are very similar to those of $LiFePO_4$, even for the high-energy surfaces. Therefore, we can conclude that for clean and stoichiometric surfaces of the olivine structure $LiMPO_4$ (M = Fe, Mn), the surface energies are largely controlled by the coordination loss on the surfaces, and the effect of the chemistry difference between Fe and Mn on the surface energies is limited. For $LiFePO_4$, the coordination loss of Fe was found to be the most important contribution to the surface energy.[10] We believe that this argument also applies for the surfaces of $LiMnPO_4$.

Given that in most orientations the surface energy of $LiMnPO_4$ is very close to the value for $LiFePO_4$, it is not surprising that the Wulff shape for $LiMnPO_4$ in this work looks quite similar to the one obtained for $LiFePO_4$ (see Fig. 11 of Ref. 10). However, compared to the Wulff shape for $LiFePO_4$, the (210) surface of $LiMnPO_4$ now appears in the equilibrium shape and replaces the edge shared by the (010) and (100) surfaces (see Fig. 1 in this work). This surface was also suggested to be one of the high-index surfaces that might appear in the Wulff shape of $LiFePO_4$ when more high-index surfaces are included.[10] Note that the surface energy of (011) is calculated to be 0.67 J/m^2 for $LiMnPO_4$ compared to 0.76 J/m^2 for $LiFePO_4$. While surface energies in other directions of $LiMnPO_4$ do not deviate too much from the numbers for $LiFePO_4$, the surface energy decrease of about 0.09 J/m^2 in the [011] orientation exposes this surface more in the Wulff shape of $LiMnPO_4$.

A significant uncertainty in applying these surface energies to real $LiMPO_4$ (M = Fe or Mn) comes from our assumption of stoichiometry on the surfaces. In reality, the loss of Li (e.g., in water during hydrothermal synthesis), oxygen, and/or OH absorption at the undercoordinated surface sites will modify the surface energies, and as a result the equilibrium particle morphology. The energy of a nonstoichiometric surface is not a material constant, but depends on the external chemical potential of the species that creates the off-stoichiometry, and as such, can only be studied for specific situations (e.g., in water or in a particular oxygen environment).

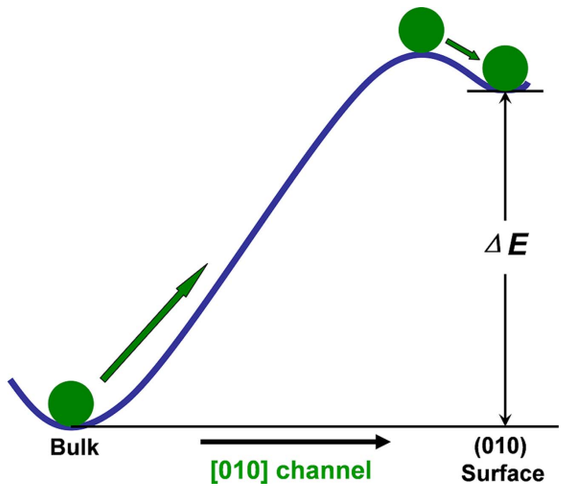

Figure 2. (Color online) Schematic drawing of the energy landscape for the Li migration along the [010] diffusion channel. The energy difference (ΔE) between the bulk Li sites and the Li sites in the outermost (010) surface layer is about 0.8 eV for $LiMnPO_4$.

Surface potentials and implications for the delithiation mechanism of nano-$LiMnPO_4$.— Among the six surfaces that appear in the Wulff shape of $LiMnPO_4$, the (010) surface has the lowest redox potential, about 0.8 V lower than the bulk value, indicating that it is energetically favorable to extract Li first from this surface. This result is consistent with what was found for $LiFePO_4$, though the difference from the bulk value is larger for $LiMnPO_4$. Therefore, one can expect that the Li extraction for $LiMnPO_4$ nanoparticles is also inhomogeneous: Li will be preferentially extracted first from the (010) surface. There are significant differences with $LiFePO_4$ for the other surfaces. While in $LiFePO_4$ the surfaces orthogonal to (010) almost all have a potential above the bulk extraction potential, in $LiMnPO_4$ all surfaces, except for (100) and (011), are below the bulk potential. Hence, while $LiFePO_4$ plates with [010] orientation will have a lithiated edge when the core is delithiated, this is unlikely to be the case for $LiMnPO_4$. We have speculated[10] that the surface regions are responsible for the electrochemical capacity that has been observed[23] above and below the bulk potential in nano-$LiFePO_4$. If this is the case, then $LiMnPO_4$ would behave differently from $LiFePO_4$ in the nanoregime. While the excess capacity of $LiFePO_4$ will be found below and above the bulk potential, in $LiMnPO_4$ it will be mainly distributed below the bulk potential. A careful comparison of the capacity outside the two-phase region for $LiFePO_4$ and $LiMnPO_4$ may therefore give some insight into whether it originates from the surfaces or from the elastic effects on the miscibility gap.[8]

The (010) surface is the most important surface, as it directly gives access to the [010] channels along which Li diffuses through the olivine structure. For both $LiFePO_4$ and $LiMnPO_4$ the potential to delithiate the (010) surface is well below the bulk potential, though the difference between bulk and surface is larger in $LiMnPO_4$ (0.8 V) than in $LiFePO_4$ (0.6 V). This indicates a significant barrier for Li to cross through the (010) surface layer (Fig. 2). Even though this barrier has to be crossed only once upon charge and discharge, the fact that it is several hundred meV larger than the Li hopping barrier in the bulk[9] likely makes it the rate-limiting factor for all but the largest particle sizes. Moreover, this energy barrier in $LiMnPO_4$ is 0.2 eV higher than in $LiFePO_4$, which may explain why the kinetics of $LiMnPO_4$ is so much slower than for $LiFePO_4$. Assuming the same prefactor for the activated surface crossing in both materials, the difference in activation energy (200 meV) accounts for a rate difference of $\exp(200\ \text{meV}/k_BT) \approx 2000$ at room temperature. If the surface potential is the rate-limiting factor, then it becomes likely that other surfaces such as (011) and (210) allow for a faster access to the bulk because they have a lithiation potential much closer to the bulk value. However, if diffusion in the bulk is truly one-dimensional,[9] then these surfaces only give access to the part of the bulk material for which the [010] channels exit at these surfaces.

Conclusions

Using first-principles calculations, we investigate surface energies, equilibrium morphology, and surface redox potentials for $LiMnPO_4$. Low-energy surfaces are found in the (100), (010), (011), (101), (201), and (301) directions. The first five surfaces appear in the Wulff shape of $LiMnPO_4$, together with the (210) surface. The dominating surfaces in the Wulff shape are (010), (011), and (201). Most of the surfaces in the Wulff shape have a Li redox potential lower than the bulk value, except for (100) and (011). The (010) surface has the lowest Li redox potential; therefore, Li is expected to be extracted first from this surface. However, the large difference between the Li redox potential in the (010) surface layers and the bulk creates a high energy barrier for Li in the bulk to diffuse out of the particle. This energy barrier may need to be lowered to improve the Li migration rate for $LiMnPO_4$, particularly at a small particle size where the surface effects become prominent. Our results indicate the importance of considering surface effects when investigating the thermodynamics and kinetics of nanoscale electrode materials.

Acknowledgments

This work was supported by the Assistant Secretary for Energy Efficiency and Renewable Energy, Office of FreedomCAR and Vehicle Technologies of the U.S. DOE under contract no. DE-AC03-76SF00098, via subcontract nos. 6517748 and 6517749 with the Lawrence Berkeley National Laboratory. We would like to acknowledge the support from the Center for Materials Science and Engineering, MIT, and the NSF MRSEC program of the NSF under contract no. DMR 02-13282. Additional computation resources were provided by the National Partnership for Advanced Computing Infrastructure (NPACI).

Massachusetts Institute of Technology assisted in meeting the publication costs of this article.

References

1. C. Delacourt, P. Poizot, M. Morcrette, J. M. Tarascon, and C. Masquelier, *Chem. Mater.*, **16**, 93 (2004).
2. M. Yonemura, A. Yamada, Y. Takei, N. Sonoyama, and R. Kanno, *J. Electrochem. Soc.*, **151**, A1352 (2004).
3. N. H. Kwon, T. Drezen, I. Exnar, I. Teerlinck, M. Isono, and M. Graetzel, *Electrochem. Solid-State Lett.*, **9**, A277 (2006).
4. H. S. Fang, L. P. Li, and G. S. Li, *Chem. Lett. (Jpn.)*, **36**, 436 (2007).
5. T. R. Kim, D. H. Kim, H. W. Ryu, J. H. Moon, J. H. Lee, S. Boo, and J. Kim, *J. Phys. Chem. Solids*, **68**, 1203 (2007).
6. A. Yamada and S. C. Chung, *J. Electrochem. Soc.*, **148**, A960 (2001).
7. C. Delacourt, L. Laffont, R. Bouchet, C. Wurm, J. B. Leriche, M. Morcrette, J. M. Tarascon, and C. Masquelier, *J. Electrochem. Soc.*, **152**, A913 (2005).
8. N. Meethong, H. Y. S. Huang, S. A. Speakman, W. C. Carter, and Y. M. Chiang, *Adv. Funct. Mater.*, **17**, 1115 (2007).
9. D. Morgan, A. Van der Ven, and G. Ceder, *Electrochem. Solid-State Lett.*, **7**, A30 (2004).
10. L. Wang, F. Zhou, Y. S. Meng, and G. Ceder, *Phys. Rev. B*, **76**, 165435 (2007).
11. F. Zhou, T. Maxisch, and G. Ceder, *Phys. Rev. Lett.*, **97**, 155704 (2006).
12. L. Laffont, C. Delacourt, P. Gibot, M. Y. Wu, P. Kooyman, C. Masquelier, and J. M. Tarascon, *Chem. Mater.*, **18**, 5520 (2006).
13. P. E. Blöchl, *Phys. Rev. B*, **50**, 17953 (1994).
14. G. Kresse and J. Furthmüller, *Phys. Rev. B*, **54**, 11169 (1996).
15. L. Wang, T. Maxisch, and G. Ceder, *Phys. Rev. B*, **73**, 195107 (2006).
16. F. Zhou, M. Cococcioni, C. A. Marianetti, D. Morgan, and G. Ceder, *Phys. Rev. B*, **70**, 235121 (2004).
17. V. I. Anisimov, J. Zaanen, and O. K. Andersen, *Phys. Rev. B*, **44**, 943 (1991).
18. V. I. Anisimov, F. Aryasetiawan, and A. I. Liechtenstein, *J. Phys.: Condens. Matter*, **9**, 767 (1997).
19. S. L. Dudarev, G. A. Botton, S. Y. Savrasov, C. J. Humphreys, and A. P. Sutton, *Phys. Rev. B*, **57**, 1505 (1998).
20. G. H. Li, H. Azuma, and M. Tohda, *Electrochem. Solid-State Lett.*, **5**, A135 (2002).
21. A. Christensen and E. A. Carter, *Phys. Rev. B*, **58**, 8050 (1998).
22. G. Wulff, *Z. Kristallogr. Mineral.*, **34**, 449 (1901).
23. N. Meethong, H. Y. S. Huang, W. C. Carter, and Y. M. Chiang, *Electrochem. Solid-State Lett.*, **10**, A134 (2007).